Experimental Study of Dynamic Strain for Gear Tooth using Fiber Bragg Gratings and Piezoelectric Strain Sensors

Yongzhi Qu[1], Liu Hong[1], Xixin Jiang[1], Miao He[2], David He[2,1], Yuegang Tan[1], Zude Zhou[1]

[1]*School of Mechanical and Electronic Engineering, Wuhan University of Technology, Wuhan, Hubei, 430070, China*
{quwong, hongliu, ygtan, zudezhou} @whut.edu.cn, jiangxixin2006@163.com

[2]*Department of Mechanical and Industrial Engineering, University of Illinois at Chicago, Chicago, IL, 60607, USA*
{mhe21, davidhe }@uic.edu

ABSTRACT

It has always been a critical task to understand gear dynamics for gear design and condition monitoring. Many gear models have been proposed to simulate gear meshing dynamics. However, most of the theoretical models are based on simplified gear structure and may contain approximation errors. Direct measuring of gear strain is important to gear design validation, load analysis, reliability assessment, gear condition monitoring, etc. Most of the existing studies of tooth strain measurements are performed under static load condition. In this paper, we investigate new measuring techniques of using fiber Bragg grating (FBG) sensor and piezoelectric strain for gear dynamic strain measurement. We conduct gear dynamic strain measurement under both low speed and normal speed condition on an industrial gearbox with relatively small module gears. Multi-combinations of speed and load conditions of the gearbox are tested and the results are discussed and analyzed. We analyze multiple factors that affect the tooth root stress, including speed, load, extended tooth meshing, etc. It is found that under low operation speed range, the tooth root strain is mainly determined by the torque, while in the mediate to high speed range, the tooth root strain is jointly affected by speed and torque. Extended tooth contact is shown in the measurement results with strong evidence. It conforms with earlier founding that the transmission error and dynamic load factor are overestimated while the operation smoothness are underestimated for spur gear under heavy load. The measured stains are also compared with numerical simulation.

1. INTRODUCTION

Gearboxes are among the most commonly used transmission components. Gear dynamics and behaviors have attracted many research attentions. In most existing literatures, investigations over gear dynamics were focused on simulation and numerical modeling. Typically, gear meshing dynamics are evaluated by computing the time varying meshing stiffness followed by analyzing gear vibration response. While theoretical analysis provides fundamental understandings of gear behaviors, there are also certain limitations. First of all, gear dynamics involves high level of nonlinearities and high order non-stationary characteristics. Contact loss, frictional effects, base stiffness, load and velocities effect, and assembly errors, etc., all affect the dynamics of gear meshing. Existing numerical models still fall short to incorporate multiple factors and therefore more sophisticated gear models are demanded. In essence, an exact analytical model to capture the overall complex gear dynamic response is inaccessible. Second, in order to validate the developed model in practice, dynamic meshing behaviors are usually fed into a set of differential equations which are used to describe the dynamic response of the gearing systems. In many cases, the dynamic response would be modeled as vibration. However, vibration as the second derivative of displacement is an indirect reflection of the excitations in gears and cannot be accurately measured due to complex signal transmission path. On the other hand, strain is a more straight measurement of material deformation and can be correlated directly with gear meshing stiffness. In this paper, experimental measuring of gear dynamic strain is proposed for gear meshing stiffness analysis.

With regard to gear condition monitoring, strain measurements are also more suitable for incipient fault diagnostics. Incipient gear faults typically would not affect the function of the gearbox and the fault feature can be hidden in the noise, and therefore hard to detect. However, an incipient gear fault may evolve rapidly into cascading catastrophic failure if left undetected. Incipient faults include micro-crack, surface smearing, and local gear profile worn, etc. While vibration based monitoring techniques is easier to implement in-situ for rotating machines, it suffers from noise and modulation effect when the signals are transmitted through complex signal paths. As reported in [1], it is difficult to detect incipient faults based on dynamic vibration analysis. On the other hand, Yoon et al. [2] reported that strain signals are more sensitive to planetary gear fault compared with vibration signals. It is known that the tooth crack or tooth pitting can be reflected by time-varying mesh stiffness and will further lead to excessive localized strain [3]. Since strain is a direct

measure of deformation of the gear teeth and reflects the mesh stiffness, strain variation can be used to detect incipient fault in much earlier stage.

2. LITERATURE REVIEW

Gear dynamics have always been a popular research area. Parker et al. [4] studied the model of non-linear dynamic response of a spur gear pair to reveal complex non-linear phenomena. The model featured a detailed contact analysis at each time step as the gears roll through the meshing line to calculate dynamic mesh forces. While the computational results agreed well with the experimental results, the authors reported that some counterintuitive findings: when the expected more accurate torque dependent stiffness curves were used, the non-linear behavior was suppressed and conflicted with high torque experiment results. The conclusions indicated that the optimal treatment of time-varying mesh stiffness, contact loss, frictional effects, etc., remains unsettled. Bartelmus [5] studied the torsional and lateral vibration model using mathematical modeling and computer simulations. Eritenel and Parker [6] studied Three-dimensional nonlinear vibration of gear pairs. Howard et al. [7] proposed a simplified gear dynamic model to explore the effect of friction on the resultant gear case vibration. Simulation results in the presence of friction and tooth crack on torsional mesh stiffness are shown to demonstrate the effect of frictional force. Jia and Howard [1] compared localized spalling and crack damage from dynamic modeling of spur gear vibrations. It is concluded that the amplitude and phase modulation of the coherent time synchronous vibration signal average can be effective in differentiating localized tooth spalling and crack damage. However, dynamic response is less effective with minor crack and profile error. Khabou [8] focused on spur gear dynamic behavior in transient regime. The dynamic behavior and external response of a single stage spur gear reducer in transient regime is studied with numerical model and experimentally investigated at different rotating velocities. They concluded that in the case of driving the transmission by a combustion engine, spectral analysis of the vibration signals may be insufficient to describe the frequency content of the response signals and a time-frequency analysis may be required to study transient regimes. Transient meshing performance analysis is also investigated using explicit dynamic finite element analysis (FEA) by Hu et al. [9] . They proposed a simulation method to study the relationships between the transient meshing performance and modification coefficient or helical angle of gears.

Recently, there are several papers that aim to measure gear mesh stiffness via experimental methods. Yesilyurt et al. [10] proposed to measure gear tooth stiffness reduction of spur gears under wear condition for severity assessment. Due to the difficulties in directly measuring the gear tooth stiffness, an experimental procedure based on the modal analysis is developed to assess the severity of the gear tooth damage. A lumped mass model was constructed to validate the experimental results. However, the method proposed was an offline testing method with the gear taken out and held static, which limited its application. Photoelasticity technique was tested by several paper for gear mesh stiffness investigation. Pandya and Parey [11] studied the effect of cracked gear fault on the tooth mesh stiffness. Both healthy gear and gears with different level of crack were tested in the study. It is proved that Photoelasticity technique polycarbonate is able to reflect gear teeth mesh stiffness variation in the presence of crack. Similarly, the experiments performed is more suitable for offline testing scenarios since it is performed on open-gear. Besides, the tested gear is made of polycarbonate birefringent material other than steel materials. Another attempt with photoelasticity to evaluate gear contact stress were reported by Frankovský et al.[12]. It is suggested that the determination of the stress state in the contact area of two bodies cannot be based only on theoretical solutions. Raghuwanshi and Parey [13] further measured gear mesh stiffness using strain gauge sensors. Strain around the tooth root were measured for both healthy and cracked teeth. Then, the measured strain was transformed into mesh stiffness. The measured mesh stiffness was compared with theoretical calculation. Overall, it indicated that strain measurement can be used for gear mesh stiffness calculation. Patil et al. [14] studied the application of using strain gauge for tooth contact strain and stress measurements. The strain gauge was mounted around the pitch line contact where the maximum contact strain is considered to lie. They concluded that strain gauges provided a proof that the effect of friction on gear contact stresses is significant and cannot be neglected. However, in the experimental, they changed the torque to simulate different levels of friction. In that case, the friction is not the only variable that affects the results.

In sum, experimental investigations are equally important as theoretical calculation for gear design evaluation and stress analysis. Although many attempts have been made towards gear strain measurements, an on-line measurement method for industrial gears is still urgently needed.

3. FIBER BRAGG GRATING SENSORS

Fiber Bragg grating (FBG) sensor is a type of distributed Bragg reflector engraved in a short segment of optical fiber that reflects particular wavelengths of light and transmits all others. FBG sensors use optic fibers as both the sensing element and the media of relaying signals. FBG optic sensors have been widely used in static structure health monitoring [15]. FBG optic sensors have the advantages of light and small, multi-point distributed and synchronized. FBG optic sensors can be used to measure multiple physical properties through a single fiber at multiple locations. Owing to its sensing principle, FBG

optic sensors can measure strain and temperature concurrently. Recent attempts have been made by using FBG optic sensors for machinery fault diagnostics. However, as reported in [16][17], the FBG optic sensors were used like vibration sensors to collect vibration signals on the cases of gearboxes. To the best of our knowledge, no research has been done on using FBG optic sensors to measure distributed gear dynamic strain directly.

In FBG measurements, strain and temperature can be correlated with the change of reflected wavelength. The sensing principle of FBGs can be expressed in the following formula:

$$\frac{\Delta\lambda}{\lambda} = k_\varepsilon \cdot \varepsilon + k_T \cdot \Delta T \quad (1)$$

where $\frac{\Delta\lambda}{\lambda}$ is the relative change of the reflected wavelength, k_ε is the coefficient of strain and k_T is the thermal expansion coefficient, and ε and ΔT are the applied strain and the change in temperature, respectively. Since in this paper our main focus is the strain, the term containing temperature will be removed by applying a low pass filter to filter out the slowly increasing or decreasing trend.

In the proposed methods, FBG optic sensors are mounted on gear end face directly to measure dynamic strain. Detailed measurement settings will be introduced in Section 5.

4. NUMERICAL SIMULATION

In order to compare the experimental results, numerical simulation were conducted on the tested gearbox. The gear parameters are listed in Table 1.

Table 1. List of parameters for gear under testing

Gear parameter	Driving gear	Driven gear
Tooth number	40	72
Module	3 mm	3 mm
Base circle diameter	112.763 mm	202.974 mm
Pitch diameter	120 mm	216 mm
Pressure angle	20°	20°
Addendum coefficient	1	1
Coefficient of top clearance	0.25	0.25
Diametral pitch	8.4667	8.4667
Engaged angle	19.7828°	19.7828°
Circular pitch	9.42478 mm	9.42478 mm
Addendum	4.5 mm	3.588 mm
Dedendum	2.25 mm	3.162 mm
Addendum modification coefficient	0.5	0.196
Addendum modification	1.5 mm	0.588 mm
Fillet radius	0.9 mm	0.9 mm
Tooth thickness	5.8043 mm	5.1404 mm
Tooth width	85 mm	85 mm
Theoretical center distance	168 mm	168 mm
Actual center distance	170.002 mm	170.002 mm

Using the given parameters, gear dynamic strain was calculated with regards to dangerous cross-section. The dangerous cross section is determined by using the Hofer's 30 degree tangent method [18]. The calculation follows typical industrial standard of gear strain evaluation similar to AGMA standard, which is introduced in the following steps:

First of all, consider the gear teeth using the cantilever beam model, the tensile stress on tooth root can be computed as the lateral component σ_w of the meshing force F_t,

$$\sigma_w = \frac{F_t}{bm_n} Y_F \quad (2)$$

$$Y_F = \frac{6\left(\frac{h_{Fe}}{m_n}\right)\cos\alpha_{Fen}}{\left(\frac{S_{Fn}}{m_n}\right)^2 \cos\alpha_n} \quad (3)$$

where, Y_F represents the gear tooth shape coefficient, b is tooth width, m_n is the normal module.

To consider the effect of the tooth root stress contraction, adding stress correction coefficient Y_S and Helix angle factor Y_β, we have .

$$\sigma_{F0} = \sigma_w Y_S Y_\beta = \frac{F_t}{bm_n} Y_F Y_S Y_\beta \quad (4)$$

Finally, we add dynamic load coefficient, gear use coefficient and load distribution coefficient to include the effect of operation condition and double tooth contact, Equ. (4) extends to,

$$\sigma_F = \sigma_{F0} K_A K_V K_{F\beta} K_{F\alpha} \quad (5)$$

If we rewrite Equ.(4) and Equ. (5), we get

$$\sigma_F = \frac{F_t}{bm_n} Y_F Y_S Y_\beta K_A K_V K_{F\beta} K_{F\alpha} \quad (6)$$

where, K_V is dynamic load coefficient, K_A gear use coefficient, $K_{F\alpha}$ is the load coefficient between gear teeth and $K_{F\beta}$ the face load distribution coefficient.

Using Equ. (6), we calculate the tooth root stress with regards to dangerous cross section during tooth meshing, the stress is calculated and plotted in Figure 1. It can be seen that in the numerical calculation, the strain transition stage are clearly separated into three zones, the first double tooth contact zone (DTCZ), single tooth contact zone (STCZ) and the second double tooth contact zone (DTCZ), respectively. Further, in the first double tooth contact zone, the bending stress gradually increase and reach maximum when initially enters the single contact zone; then the bending stress starts to decrease until it exist meshing.

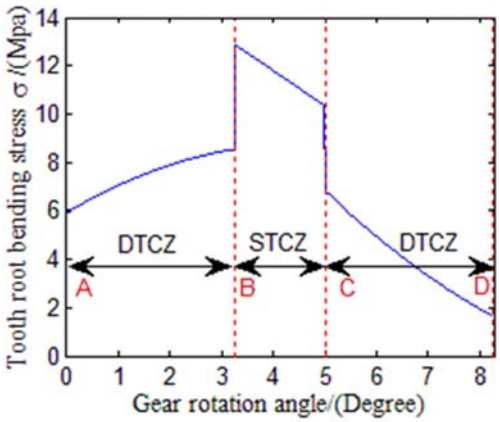

Figure 1. Dynamic stress transition process during gear meshing

The contact ratio under the given gear parameters can be calculated as

$$\varepsilon_\alpha = \frac{1}{2\pi}[z_1 * (\tan(a\cos(\frac{r_{b1}}{r_{a1}})) - \tan\alpha') + z_2 * (\tan(a\cos(\frac{r_{b2}}{r_{a2}})) - \tan\alpha')] = 1.6537$$

The ratio between double tooth contact zone (AB) and single tooth contact zone(BC) is calculated as: AB:BC = 0.6537:0.3463 = 1.8877.

The computed value will be compared with measuring results in the experimental section.

5. EXPERIMENTAL WORK

5. 1 Test rig

The gear strain measurement experiments were performed on an industrial standard gearbox installed in an electronically closed transmission test rig. The overall test rig is showed in Fig. 2.

The gearbox test rig includes two 45 kW Siemens servo motors. One of the motors can act as the driving motor while the other can be configured as the load motor acting as a generator. The configuration of the driving mode is flexible. Compared with traditional open loop test rig, the electrically closed test rig is economically more efficient, and can virtually be configured with arbitrary load and speed specifications within rated power.

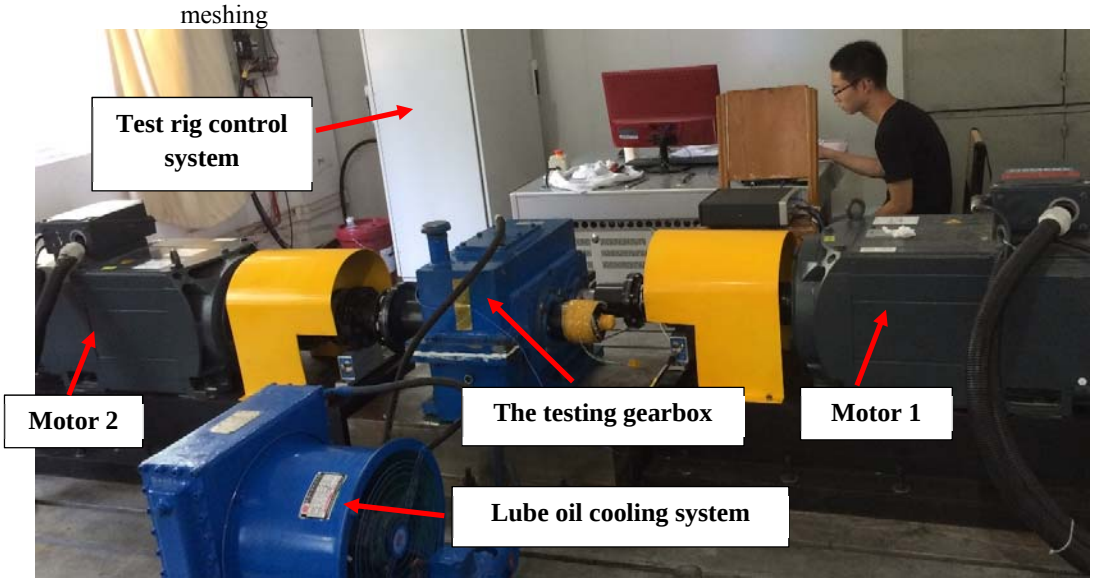

Figure 2. Experiment test rig for gearbox dynamic mesh stiffness analysis

The testing gearbox is a one stage gearbox with spur gears. The gearbox has a speed reduction rate of 1.8:1. The input driving gear has 40 teeth and the driven gear has 72 teeth. The geometric model of the gearbox is shown in Fig. 3.

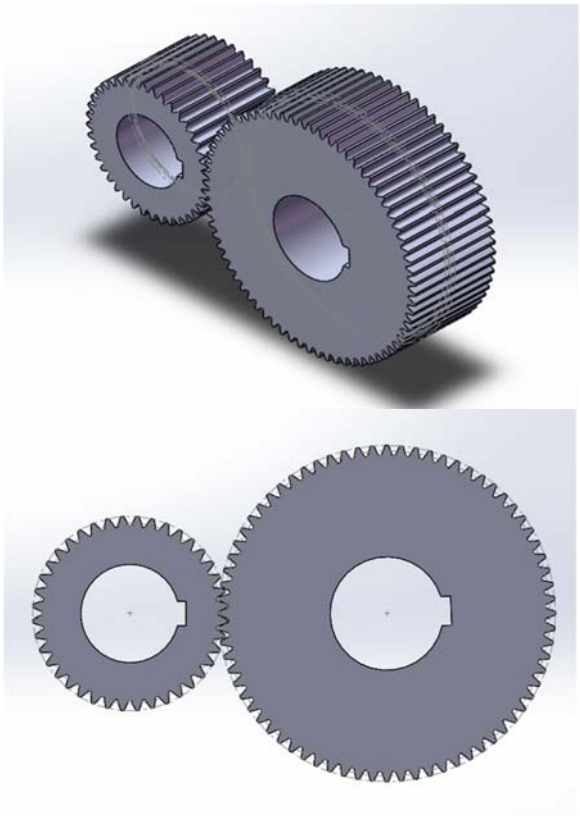

Figure 3. 3D model of the spur gear under test

5.2 Sensor deployment specifics

All the strain measurements were made on the output driven gear with 72 teeth. FBG sensors with a grating length of 5 mm at an interval of 58 mm along the optic fiber were customized to measure distributed gear strains. There are a total of ten FBG sensors attached on the driven gear. Nine out of ten FBGs were attached to the tooth root of gear-end-dace along the base circle for dynamic strain measurements, while the tenth FBG is bonded on the gear output shaft for torque measurements. Approximately, one FBG sensor was bonded to the tooth root for every seven teeth.

Together with the FBG sensors, two piezoelectric strain sensors from PCB® Piezotronics were also attached on the tooth root of gear end face in between the FBG sensors. The details of the strain measurement configuration are shown in Fig. 4. Both the FBG signal and piezoelectric signal were collected through rotary joints. The FBG signals were sampled at 5 KHz sampling rate, while the piezoelectric strain signals were sampled at 20.48 KHz.

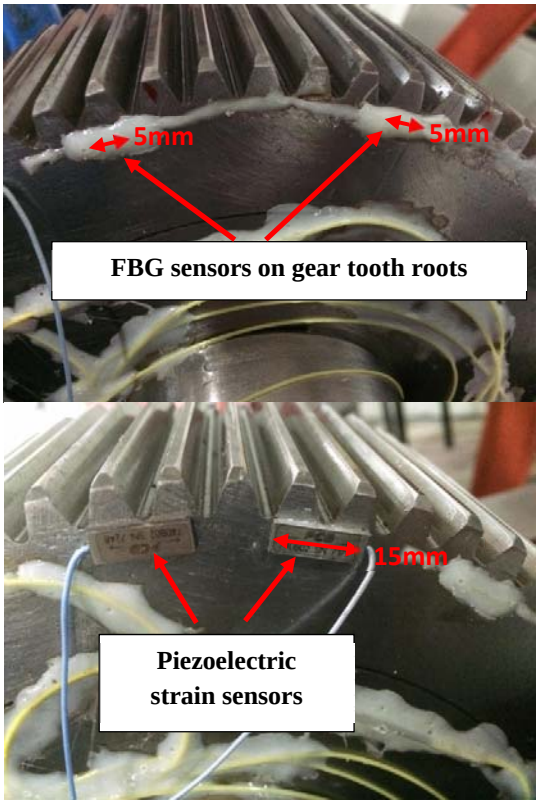

Figure 4. Sensor deployment

5.3 Testing Condition

Gearbox under various running condition were tested and the signal collected. The tested operation conditions are listed in Table 1. and Table 2.

Table 1. Operation condition of the experiments (low speed)

Speed (rpm) / Torque (Nm)	100	200	300	400	500	600	700	800	900	1000
50	●	●	●	●	●	●	●	●	●	●
100	●	●	●	●	●	●	●	●	●	●
200	●	●	●	●	●	●	●	●	●	●
300	●	●	●	●	●	●	●	●	●	●
400	●	●	●	●	●	●	●	●	●	●
500	●	●	●	●	●	●	●	●	●	●

Table 2. Experimental operation condition (median to high speed)

Speed (rpm) / Torque (Nm)	1200	1500	1800	2100	2400
50	●	●	●	●	●
100	●	●	●	●	●
200	●	●	●	●	●
300	●	●	●	●	●

6. MEASUREMENT RESULTS

The results were analyzed in the following perspectives: (1) Overall strain measurements from FBG sensors and piezoelectric strain sensors. (2) Strain amplitude variation under different speed and load conditions. (3) Dynamic strain behavior analysis.

6.1 Overall gear strain evaluation

A typical measurement of the strain signal using FBG sensors is shown in Figure 6. Figure. 6 (a) shows the strain bursts measured in 2s. Each burst represents one gear mesh period in a revolution. Figure. 6 (b) shows two of the bursts zoomed. It can be seen that FBG signals clearly recorded the dynamic transition of the strain variation process. A comparison with the signals collected with piezoelectric strain sensors is shown in Figure. 7. Both FBG and piezoelectric sensors measurements display the same pattern. It is noticed that the strain from piezoelectric sensors has a much smaller amplitude compared that of the FBG sensors. This is likely caused by that the size of piezoelectric sensors (15 mm) is much larger than that of the FBG sensors (5 mm) in the sensitive direction, which lead to a smaller average of strain in a broader area.

It is found that for each tooth mesh process, the tensile strain first gradually picks up, followed by a compressive strain peak and a tensile strain peak, and then another compressive peak which gradually diminish after the tooth exist meshing. Similar phenomena were also observed in early report [19], which utilized strain gages at tooth fillet and tooth root. A possible explanation for the strain transition is given below. It is assumed that both the FBG and the piezoelectric strain sensor mainly measure the bending stress as they are attached along the transverse direction of the tooth along dangerous cross section. Since the measuring tooth is on the driven gear, as the measuring tooth come closer to the meshing position, the neighbor teeth generate the tensile strain in the upcoming meshing area of the gear rim and affected the measured tooth. This explains the gradually picking up of the tensile strain. When the measured tooth initially enters meshing, the last tooth is still engaged and this is the first double-tooth contact zone. On entering the double tooth-contact zone, the overall tooth stress is compressive. As the tooth increasingly picks up force, the tensile strain takes dominant role all the way into single-tooth contact zone, where the tensile strain reaches the maximum. Then, the tensile stress continuously drops and gives way to compressive stress when the next tooth takes dominant role. After the measured gear tooth exists meshing area, the compressive stress gradually decrease to zero.

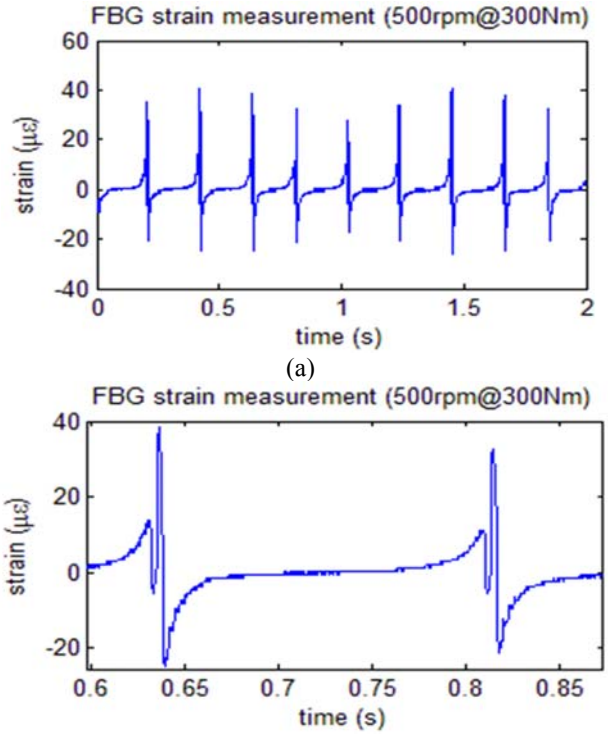

Figure 6. Strain measurement with FBG sensors (a) strain peaks in 2s (b) enlarged 2 peaks

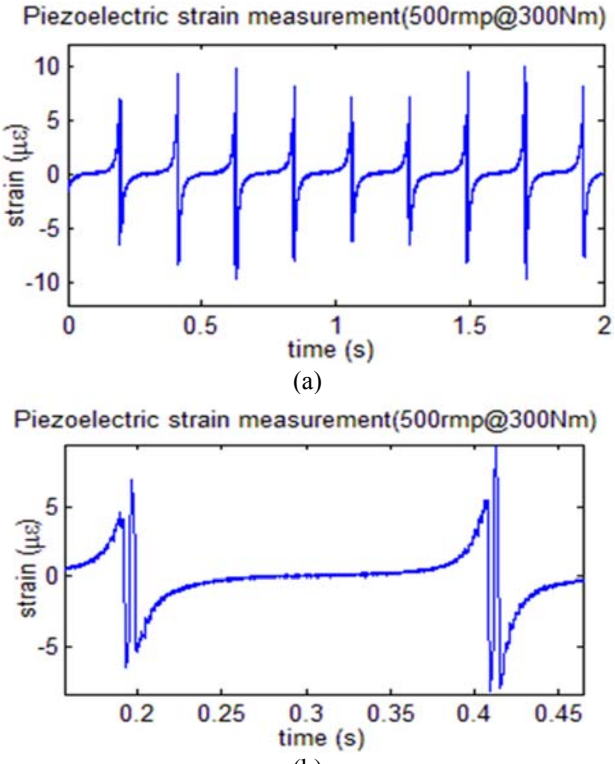

Figure 7. Strain measurement with piezoelectric sensors(a) strain peaks in 2s (b) enlarged 2 peaks

6.2 Amplitude measurement and comparison

Using the amplitude of one of the FBG sensors as example, we evaluate the relationship between strain amplitude and speed and load. All of the shown results are averaged over 5 measurements, each containing 3s of signals. The fluctuation between different sample is negligible, which means the strain measurements are relatively stable. The amplitude comparison results of the low speed range are given in Figure 9, where different color indicate different torques.

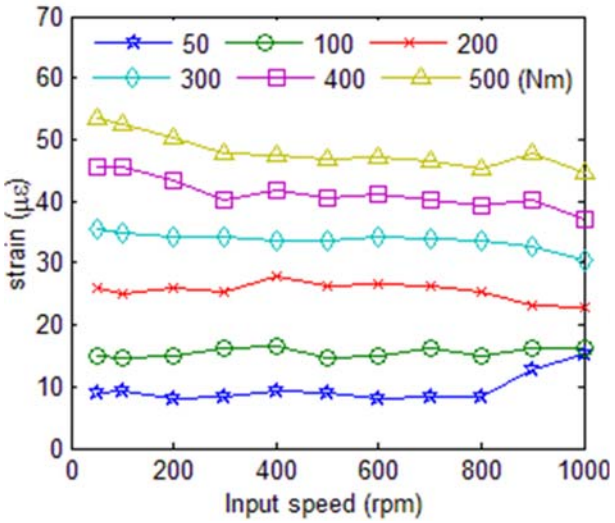

Figure 9. FBG strain amplitude under varying speed and load

In the low speed range, torque rating from 50 Nm to 500 Nm were tested under each speed. Due to the power limitation of the motors, we only tested 50 to 300Nm above 1000 rpm as shown in Table 2. It can be seen from Figure 9 that the tooth root strains increase steadily with torque. To visualize the increasing trend with torque, this is further shows in Figure 10. It is shown that strain amplitude increases almost linearly with torque. However, the strains remain almost constant under different speeds in the range of 50 rpm to 1000 rpm. When the torque is 50Nm, the strain increase slightly with speed at 900 and 1000rpm. For torque higher than 50Nm, the strain increase is not significant with the increasing of speed within 1000rpm. Overall, the strain is not sensitive to speed in the low speed range as shown in Figure 9. The results of the full speed range is shown in Figure 11. It is shown that when the input speed is larger than 1000 rpm, the amplitude of strain is determined by both speed and torque. In some cases, strains can be higher with lower applied torque than higher applied torque. In sum, the strain amplitude in higher speed range is not strictly in line with speed and torque though determined by both.

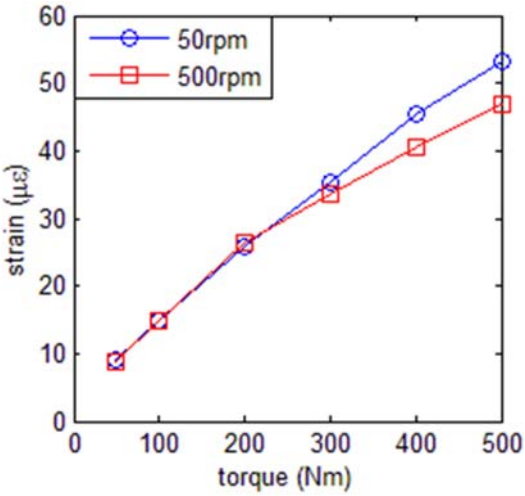

Figure 10. Relationship between strain and torque

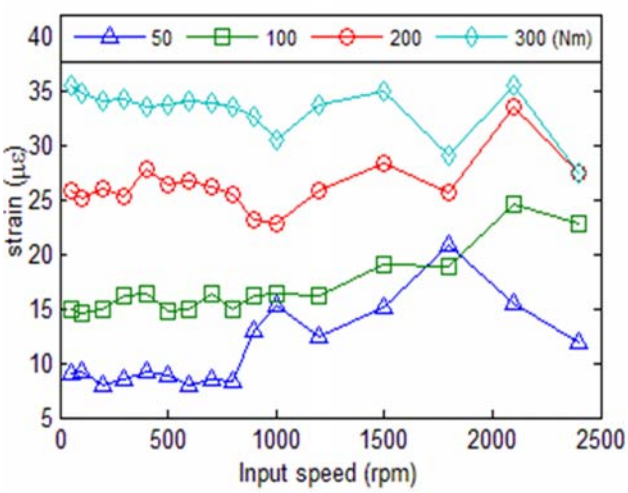

Figure 11. Full range strain-speed relationship

6.3 Dynamic meshing strain

One of the main purpose of the strain measurement is to understand the gear strain dynamic process. To examine the stress transition process, again we take the measurement of 500 rpm at 300Nm as an example and we further enlarged the burst in Figure 6 and Figure 7, which is shown in Figure 12. Again, both FBG and piezoelectric strain sensors display the same trend.

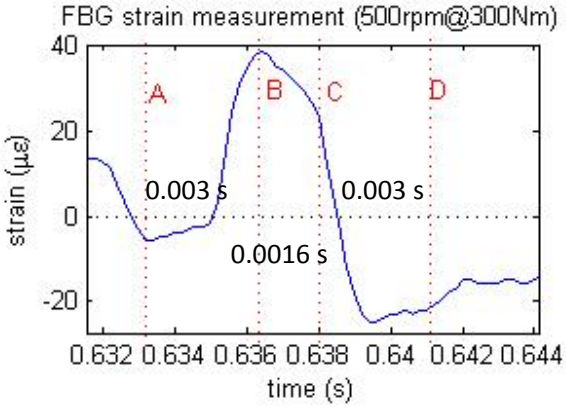

(a)

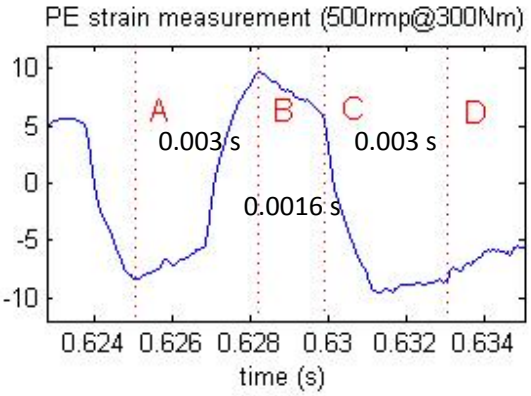

(b)

Figure 12. Enlarged FBG strain measurement (a), Enlarged piezoelectric strain measurement (b)

Compare with the simulation result in Figure 1, it can be seen that the single tooth contact zone BC can be clearly identified as well as the first and second double tooth contact zone, AB and CD. A closer look at the dynamics stress process indicate that the rising and falling trends also conform well with the simulation results. Especially, in Figure 12(b), which is the piezoelectric (PE) strain measurement, it can be seen that in the first double tooth contact zone the rising trend turns downward while in the second double contact zone the falling trend turns upward, which is exactly the same with the simulation results. However, the transition time period indicate that the total meshing time for each tooth is around 0.0076s, which is far over 0.005s computed with the gear running under 500 rpm input speed. This indicate that the contact ratio is over 2 for the spur gear tested under 300Nm torque. Further, the ratio between double tooth contact zone and single tooth contact zone is 0.003/0.0016 = 1.875, which is close to 1.8877 as calculated in section 3. However, the contact ratio is calculated as 0.0076/0.003=2.53, which means there are significant extended tooth contact during tooth meshing.

The founding can be explained by extended tooth contact which has been reported in [19,20]. It was argued in [19] that by ignoring the extended tooth contact, the zone of tooth contact and the average tooth mesh stiffness are underestimated, while the individual tooth load is overstated, especially for heavily loaded gears. The static transmission error and dynamic load of heavily loaded, low-contact-ratio spur gears are also overestimated when the effect of tooth flexibility is ignored. It is further reported in [20], under large torque, due to the flexibility of the mating gear that the contract ratio can increase significantly and in some case, for spur gear, it can have 3 teeth in contact during meshing. However, both paper are based on modeling and numerical simulation. The measurement results in this paper proves that the total meshing period is significantly prolonged for each tooth. Another question remains unanswered is when extended tooth contact is taken into consideration, how to determine the actual contact ratio as well as the portion of single tooth contact zone, double tooth contact zone and possible triple tooth contact zone. This will be investigated in the future.

7. DISCUSSION

As can be seen from section 4 that both sensors could effectively reflect the dynamic transition of tooth root stress and record the details of gear dynamic strain. The following conclusions can be drawn from the experimental results:

(1) Gear teeth experience multiple tensile and compressive deformation stage during meshing. This can assist analysis of gear tooth root bending fatigue and reliability evaluation.

(2) Gear tooth root stress under low to mediate speed is mainly determined by the torque. However, in higher speed range, speed and torque jointly determine the stress level. The increasing of tooth root stress is not uniform with the increasing of speed and torque due to gear dynamic load and gear modal. The theoretical determination of gear load factor may not be adequate.

(3) Due to the flexibility of gear rim and teeth, the actual contract ratio is far over the theoretical value, especially under large torque. It indicates that the transmission smoothness are underestimated in theoretical analysis.

8. CONCLUSIONS

To be best of the authors' knowledge, this is the first paper that report gear dynamic strain measurement using optic fiber Bragg grating sensors as well as piezoelectric strain sensors. Existing gear dynamics analysis was based on time varying mesh stiffness. However, the modeling of time varying mesh stiffness largely depends on simplified gear model, which cannot be validated by experimental study due to limitation of measuring techniques. Previous experimental work mainly instigated static measurements of tooth root strain under load. This research measured gear dynamic strain under normal operating condition without interrupting normal gearbox operating and provide insights

for gear dynamic modeling. The results in this paper proved that extended tooth contact greatly affected the tooth root strains. Future work will include how to derive time varying mesh stiffness using experimental data.

ACKNOWLEDGEMENT

This work was partially supported by NSFC (51505353) and NSFC (51605349), and NSF of Hubei Province (2016CFB584).

REFERENCE

[1] S. Jia, I. Howard, and J. Wang, The Dynamic Modeling of Multiple Pairs of Spur Gears in Mesh, Including Friction and Geometrical Errors, *International Journal of Rotating Machinery*, Vol. 9, No. 6, pp. 437-442, 2003.

[2] J. Yoon, D. He, and B. V. Hecke, On the Use of a Single Piezoelectric Strain Sensor for Wind Turbine Planetary Gearbox Fault Diagnosis, *IEEE Transactions on Industrial Electronics*, Vol. 62, No. 10, pp.65 – 85, 2015.

[3] H. Endo, R. B. Randall, and C. Gosselin, "Differential diagnosis of spall vs. cracks in the gear tooth fillet region: experimental validation," *Mechanical Systems and Signal Processing*, vol. 23, no. 3, pp. 636–651, 2009.

[4] R.G. Parker, S.M. Vijayakar, T. Imajo, Non-linear Dynamic Response of a Spur Gear Pair: Modelling and Experimental Comparisons, *Journal of Sound and Vibration*, Volume 237, Issue 3, 2000, Pages 435-455.

[5] W. Bartelmus, Mathematical Modelling and Computer Simulations as an Aid to Gearbox Diagnostics, *Mechanical Systems and Signal Processing*, Volume 15, Issue 5, pp. 855-871, 2001.

[6] T. Eritenel, R. G. Parker, Three-dimensional nonlinear vibration of gear pairs, *Journal of Sound and Vibration*, Volume 331, Issue 15, pp. 3628-3648, 2012.

[7] I. Howard, S. Jia, J. Wang, The Dynamic Modelling of a Spur Gear in Mesh Including Friction and a Crack, *Mechanical Systems and Signal Processing*, Volume 15, Issue 5, Pages 831-853, 2001.

[8] M.T. Khabou, N. Bouchaala, F. Chaari, T. Fakhfakh, M. Haddar, Study of a spur gear dynamic behavior in transient regime, *Mechanical Systems and Signal Processing*, Volume 25, Issue 8, pp. 3089-3101, 2011.

[9] Y. Hu, Y. Shao, Z. Chen, M. J. Zuo, Transient Meshing Performance of Gears with Different Modification Coefficients and Helical Angles Using Explicit Dynamic FEA, *Mechanical Systems and Signal Processing*, Volume 25, Issue 5, pp. 1786-1802, 2011.

[10] I. Yesilyurt, F. Gu, A. D. Ball, Gear Tooth Stiffness Reduction Measurement Using Modal Analysis and Its Use in Wear Fault Severity Assessment of Spur Gears, *NDT & E International*, Volume 36, Issue 5, pp. 357-372, 2003.

[11] Y. Pandya, A. Parey, Experimental Investigation of Spur Gear Tooth Mesh Stiffness in The Presence of Crack Using Photoelasticity Technique, *Engineering Failure Analysis*, Volume 34, December 2013, Pages 488-500.

[12] P. Frankovský, O. Ostertag, F. Trebuňa, E. Ostertagová , M. Kelemen, Methodology of Contact Stress Analysis of Gearwheel by Means of Experimental Photoelasticity, *Applied Optics*. 55(18), pp. 4856-64, 2016.

[13] N. K. Raghuwanshi, A. Parey, Experimental Measurement of Gear Mesh Stiffness of Cracked Spur Gear by Strain Gauge Technique, *Measurement*, Volume 86, May 2016, Pages 266-275.

[14] S. S. Patil, S. Karuppanan, I. Atanasovska, Experimental measurement of strain and stress state at the contacting helical gear pairs, *Measurement*, Volume 82, March 2016, Pages 313-322.

[15] H. Guo, G. Xiao, N. Mrad, and J. Yao, Fiber Optic Sensors for Structural Health Monitoring of Air Platforms, *Sensors*, Vol. 11, No. 4, pp. 3687-3705, 2011 .

[16] J. S. Kiddy, P. D. Samuel, D. G. Lewicki, K. E. LaBerge, R. T. Ehinger, and J. Fetty, Fiber optic strain sensor for planetary gear diagnostics, NASA Glenn Res. Center, Cleveland, OH, USA, *Technical Report NASA/TM-2011-217123*, Nov. 2011.

[17] C. S. Baldwin, J. S. Kiddy, and P. D. Samuel, Towards development of a fiber optic-based transmission monitoring system, *Proc. SPIE 8026, Photonic Applications for Aerospace, Transportation, and Harsh Environment II*, 80260N, May 25, 2011.

[18] M. Savage, K.L Rubadeux and H.H. Coe, Bending strength model for internal spur gear teeth, *31st Joint Propulsion Conference and Exhibit*, San Diego,CA, U.S, July 10-12, 1995.

[19] F. B. Oswald, Gear tooth stress measurements on the UH-60A helicopter transmission, Technical Report NASA-TP-2698, E-3357, NAS 1.60:2698, United States

[20] H. H. Lin, J. Wang, F. B. Oswald, and J. J. Coy, Effect of extended tooth contact on the modeling of spur gear transmissions, 29th Joint Propulsion Conference and Exhibit, Monterey, CA,U.S.A, 1993.

[21] H. Ma, X. Pang, R. Feng, R. Song, B. Wen, Fault features analysis of cracked gear considering the effects of the extended tooth contact, Engineering Failure Analysis, Vol. 48, pp. 105-120, 2015.